Interactions of Alkyltin Salts with Biological Dithiols: Dealkylation and Induction of a Regular *β*-Turn Structure in Peptides

Bethany A. Buck, Alessandro Mascioni, Christopher J. Cramer, and
Gianluigi Veglia*

Contribution from the Department of Chemistry and the Supercomputing Institute, University of Minnesota, 207 Pleasant St. SE, Minneapolis, Minnesota 55455-0431

Received July 1, 2004; E-mail: veglia@chem.umn.edu

Abstract: Organotin compounds specifically target vicinal dithiols, thereby inhibiting the function of essential enzymes. Here, we present the NMR binding studies of trimethyltin (TMT) and dimethyltin (DMT) chlorides with a linear peptide (ILG***C***W***C***YLR) derived from the membrane protein stannin (SNN). We show that this peptide is able to dealkylate TMT and bind DMT, adopting a stable type-I *β*-turn conformation. Both the NMR data and the calculated structures indicate that the two cysteines coordinate the tin atom in a distorted tetrahedral geometry. The molecular geometries and tin coordination state were confirmed using density functional theory (DFT). In addition, NMR spectral parameters back calculated from the DFT minimized structure compared well with experimental data. These results in conjunction with studies on peptide variants (i.e., C4S, C6S, and Y7F) demonstrate unequivocally the key role of biological dithiols in both the dealkylation and binding of organotin compounds. This peptide serves as a model system for alkyltin-protein interactions and gives new insights into the biological fate of alkyltin compounds.

Introduction

Organometals are potent neurotoxic cell signaling molecules.[1,2] In particular, organotin, organolead, and organomercury compounds display the highest level of cytotoxicity. These molecules are avid ligands for the active sites of essential enzymes rich in histidines and cysteines, blocking their biological function or triggering alternative biochemical pathways.[3] Unlike organolead and organomercurial compounds, organotin derivatives are highly specific for their biological targets.[4] For example, trimethyltin chloride (TMT) and triethyltin chloride (TET) are both neurotoxins; however, they differ significantly in their biological action. TMT neurotoxicity is localized in the central nervous system (hippocampus and neocortex), while TET induces damage within the periferal nervous system (spinal cord).[5,6] This high specificity and toxicity of organotin compounds have made them ideal candidates for modeling the mechanisms of alkylmetal intoxication in mammalians, though it is only recently that attention has been focused on their biological chemistry.[7]

Organotins are composed of a tetravalent tin(IV) atom with at least one organic or aryl moiety. The toxicity of alkyltin compounds correlates directly with the number and nature of the organic groups. Trialkyltin compounds with short alkyl chains are considered the most toxic, with toxicity decreasing with increasing chain length.[8] Accidental human intoxication with trialkyltins has resulted in adverse health consequences, including memory loss, seizures, and death.[9–11] Interestingly, it has been shown that tetra- and trialkylorganotins when introduced into the environment are progressively dealkylated from polyalkyltin to monoalkyltin derivatives by unknown mechanisms. Organotin compounds, unintentionally ingested by mammals (including humans), exhibit an identical fate.[9,12] To date, it is not currently understood whether this in vivo dealkylation is directly correlated to the neurotoxic response described above.

In 1997, toxicological studies conducted with TMT intoxicated mice helped identify the 2.9 kb cDNA encoding for a relatively small membrane protein, stannin (SNN).[13–15] These researchers showed that SNN is able to trigger neuronal cell apoptosis rather than necrosis upon direct interaction with

(1) Costa, L. G.; Guizzetti, M.; Lu, H.; Bordi, F.; Vitalone, A.; Tita, B.; Palmery, M.; Valeri, P.; Silverstrini, B. *Toxicol.* **2001**, *160*, 19−26.
(2) Costa, L. G. *Annu. Rev. Pharmacol. Toxicol.* **1998**, *38*, 21−43.
(3) Chang, L. *J. Toxicol. Sci.* **1990**, *15*, 125−151.
(4) Philbert, M. A.; Billingsley, M. L.; Reuhl, K. R. *Toxicol. Path.* **2000**, *28*, 43−53.
(5) Viviani, B.; Galli, C. L.; Marinovich, M. *Neurosci. Res.* **1998**, *23*, 139−149.
(6) Aschner, M.; Aschner, J. L. *Neurosci. Biobehav. Rev.* **1992**, *16*, 427−435.
(7) Buck, B.; Mascioni, A.; Que, L.; Veglia, G. *J. Am. Chem. Soc.* **2003**, *125*, 13316−13317.
(8) Hoch, M. *Appl. Geochem.* **2001**, *16*, 719−743.
(9) Gui-Bin, J.; Qun-fang, Z.; Bin, H. *Bull Environ Contam Toxicol* **2000**, *65*, 277−284.
(10) Feldman, R. G.; WHite, R. F.; Eriator, I. I. *Arch. Neurol.* **1993**, *50*, 1320−1324.
(11) Kreyberg, S.; Torvik, A.; Bjorneboe, A.; Wiik-Larson, W.; Jacobson, D. *Clin. Neuropath.* **1992**, *11*, 256−259.
(12) Arakawa, Y.; Wada, O.; Yu, T. H. *Toxicol. Appl. Pharmacol.* **1981**, *60*, 1−7.
(13) Toggas, S. M.; Krady, J. K.; Billingsley, M. L. *Mol. Pharm.* **1992**, *42*, 44−46.
(14) Dejneka, N. S.; Patanow, C. M.; Polavarapu, R.; Toggas, S. M.; Krady, J. K.; Billingsley, M. L. *Neurochem. Int.* **1997**, *31*, 801−815.
(15) Toggas, S. M.; Krady, J. K.; Thompson, T. A.; Billingsley, M. L. *Ann. N. Y. Acad. Sci.* **1993**, *679*, 157−177.

TMT.[13-15] SNN possesses several potential TMT binding sites including 3 cysteines in positions 32, 34 and 71, and 2 histidines in positions 6 and 87, respectively.[15] Two of the cysteines (32 and 34) are highly conserved and may constitute the primary binding site for TMT, based on recent evidence that organotin compounds target vicinal dithiols over monothiols both in vivo and in vitro.[16,17]

To mimic stannin's binding site and to model the mechanism of TMT toxicity, we synthesized a 9-residue peptide (SNN-PEP) corresponding to residues 29−37 of the SNN sequence (ILGCWCYLR). This small peptide contains a CXC motif, which is common in many metal-binding proteins.[18-20] We have previously shown that this peptide is capable of binding and dealkylating trialkyltin compounds via these vicinal thiols.[7] Circular Dichroism (CD) spectra show that the free peptide is unstructured in solution and adopts an ordered conformation upon interaction with TMT. SNN-PEP binds various alkyltins with the following order of affinity: dimethyltin dichloride (DMT) > diethyltin dichloride (DET) > tripropyltin chloride (TPrT) > TET > TMT, but no binding was observed for TBT, MMT, and SnCl₄.[7]

Building on our previous work,[7] in this paper using solution NMR, ESI−MS, and DFT (density functional theory) calculations, we show that (a) TMT and DMT form identical complexes with SNN-PEP, (b) the high-resolution structure of the SNN-PEP/DMT complex solved by NMR is a well-defined β-turn, and (c) the geometry of the metal center is a distorted tetrahedron. The peptide geometry and coordination about the metal site were optimized at the density functional level of theory using a generalized gradient exchange-correlation functional method (HCTH). Density functional calculations were further employed to assist in the interpretation of NMR parameters. Organotin interactions with peptide variants, substituting serines for cysteines (C4S and C6S), were also studied by NMR to demonstrate that dithiols rather than monothiols are required for both the binding and dealkylation of trialkyltin compounds.

Experimental and Computational Section

Materials. Trimethyltin chloride, triethyltin chloride, tripropyltin chloride, and dimethyltin dichloride were purchased from Strem Chemicals (Newburyport, MA). Diethyltin dichloride was purchased from Alfa Aesar (Ward Hill, MA). All alkyltin compounds were used without further purification. Crude SNN-PEP and peptide variants were synthesized by the Microchemical Facility using standard solid-phase synthesis (University of Minnesota; Minneapolis, MN).

HPLC Purification of SNN-PEP and Peptide Variants. Crude peptide was dissolved in a solution of 50:50 acetonitrile (ACN):H₂O and separated by reversed-phase HPLC. A Hewlett-Packard 1100 series HPLC equipped with a Waters Delta Pak 15 μ C18−300 Å column (Milford, MA) was used for the separation. SNN-PEP and variants were isolated using a 1.00 mL/min flow rate and a 70 min solvent gradient of 80%B/20%A to 0%B (A: ACN/0.085% v/v trifluoroacetic acid (TFA); B: H₂O/0.1% v/v TFA). Solvent was removed under gentle N₂(g) flow and the residue redissolved in double distilled H₂O before lyophilization. Peptide purity was verified by HPLC traces and ESI−MS.

NMR Spectroscopy. NMR samples consisted of 0.8 mM peptide in 20 mM phosphate buffered saline (PBS, pH 4.0 or 6.5), 0.08 mM DTT, and 10% D₂O. Measurements were performed at 298 K on a Varian UNITY Inova 4-channel NMR spectrometer operating at 600.13 MHz. Solutions containing organotin chlorides were prepared in d₆-EtOH and titrated into the peptide sample. Water signal was suppressed by applying a WATERGATE pulse sequence.[21] For experiments carried out at a different pH, peptide/organotin solutions were titrated with a 1M solution of NaOH. Resonance assignments were performed using 2D-TOCSY (mixing times of 50 and 75 ms) and ¹H/¹H-ROESY (mixing times of 100, 200, 350, and 400 ms) experiments. NMR spectra were processed using NMRPipe.[22] TOCSY experiments were acquired with 2048 complex points in the direct dimension and 128−256 complex points in the indirect dimension. ROESY experiments were acquired with 2194 complex points in the direct dimension and 128 complex points in the indirect dimension. All spectra were processed with a cosine squared bell function, zero filled to double the size in both dimensions, and linear predicted to add 128 (TOCSY) or 160 (ROESY) additional points before Fourier transformation.

Hydrogen bonds were determined by lyophilizing the solution of SNN-PEP/DMT complex and resuspending the powder in 100% D₂O. Exchange protected amide protons were determined by using a ¹H/¹H-ROESY (mixing time 350 ms) experiment. Remaining peaks after 16 h were considered hydrogen bonded. ¹J(¹¹⁹Sn,¹³C) and ²J(¹¹⁹Sn, ¹H) were measured using the ¹H/¹³C-HMQC pulse sequence[23,24] on an Inova 4-channel spectrometer operating at 800.24 MHz. 2048 complex points and 48 complex points were acquired in the direct and indirect dimensions, respectively. The spectrum was processed using a cosine squared bell function; zero filling to double the size in both dimensions and linear prediction to extend the FID by an additional 64 points.

NMR Structure Determination. Intra- and interresidue dipolar contacts for the SNN-PEP/DMT complex were identified using a 2D-ROESY spectrum (400 ms mixing time), and the structures calculated using X-PLOR.[25] A total of 54 ROEs consisting of 35 inter- and 19 intraresidue ROEs were assigned and classified as strong (1.8−2.9 Å), medium (1.8−3.4 Å) or weak (1.8−5.0 Å) according to Wuthrich.[26] Aromatic proton and methylene ROEs were adjusted by applying pseudo-atom corrections where appropriate.[27] The DMT molecule was built into the peptide using modified scripts included in the X-PLOR-NIH package. The CH₃−Sn−CH₃ angle of the DMT molecule bound to the peptide was derived from tin-proton and tin−carbon couplings obtained from a ¹H/¹³C-HMQC spectrum for the complex using the following equations derived by Lockhart and Manders

$$\theta = 0.0161|^2J|^2 - 1.32|^2J| + 133.4^{28} \qquad (1)$$

$$|^1J| = (10.7 \pm 0.5)(\theta) - (778 \pm 64)^{29} \qquad (2)$$

where θ represents the CH₃−Sn−CH₃ angle. Remaining DMT geometry parameters were based on literature values from model compounds including, Sn−S bond lengths,[30] Sn−C bond lengths, S−Sn−CH₃ angles and S−Sn−S angles.[31]

Structures were calculated using simulated annealing from an extended structure at an initial temperature (T_i) of 1000 K with 6000

(16) Stridh, H.; Orrenius, S.; Hampton, M. B. *Toxicol. Appl. Pharmacol.* **1999**, *156*, 141−146.
(17) Nishikimi, A.; Kira, Y.; Kasahara, E.; Sato, E. F.; Kanno, T.; Utsumi, K.; Inoue, M. *Biochem J.* **2001**, *356*, 621−626.
(18) DeSilva, T. M.; Veglia, G.; Porcelli, F.; Prantner, A.; Opella, S. J. *Biopolymers (Biospectroscopy)* **2002**, *64*, 189−197.
(19) Romero-Isert, N.; Vasak, M. *J. Inorg. Biochem.* **2002**, *88*, 388−396.
(20) Vats, N.; Lee, S. F. *Microbiol.* **2001**, *147*, 653−662.
(21) Piotto, M.; Saudek, V.; Sklenar, V. J. *J. Biomol. NMR* **1992**, *2*, 661−665.
(22) Delaglio, F.; Grzesiek, S.; Vuister, G. W.; Zhu, G.; Pfeifer, J.; Bax, A. *J. Biomol. NMR* **1995**, *6*, 277−293.
(23) Muller, L. *J. Am. Chem. Soc.* **1979**, *101*, 4481−4484.
(24) Bodenhausen, G.; Ruben, D. *J. Chem. Phys. Lett.* **1980**, *69*, 185−189.
(25) Brunger, A. *X-PLOR Version 3.1 A System for X-ray Crystallography and NMR*; Yale University: New Haven, 1992.
(26) Wutrich, K. *NMR of Proteins and Nucleic Acids*; John Wiley and Sons: New York, 1986.
(27) Wuthrich, K.; Billeter, M.; Braun, W. *J. Mol. Biol.* **1983**, *169*, 949−961.
(28) Lockhart, T. P.; Manders, W.; F. *Inorg. Chem.* **1986**, *25*, 892−895.
(29) Lockhart, T. P.; Manders, W.; F. *J. Am. Chem. Soc.* **1987**, *109*, 7015−7020.
(30) Domazetis, G.; Mackay, M.; Magee, R.; James, B. *Inorg. Chimi. Acta* **1979**, *34*, L247−L248.
(31) Mohamed-Ibraham, M.; Khor, C.; Fun, H.; Sivakumar, K. *Acta Crystallogr.* **1996**, *C52*, 845−846.

high steps, 3000 cooling steps, and a step size of 5 fs to generate 100 conformers. Final structure refinement was carried out by gradually introducing van der Waals radii and Lennard-Jones potentials on the 100 structures using a T_i of 300 K, 30 000 cooling steps, and a step size of 1 fs. Eighty-one structure were selected from the 100 with zero ROE violations > 0.5 Å, zero bond violations > 0.5 Å, and no dihedral violations > 5°. Twelve lowest energy conformers were selected on basis of satisfying favorable Ramachandran angles (calculated using X-PLOR)[25] and the hydrogen bonds observed from D_2O exchange experiments. Structures were visualized using the MolMol software package.[32]

Computational Methods. Starting from the average NMR structure, molecular geometries were optimized at the density functional level of theory employing the most recent refinement[33] of the generalized gradient exchange-correlation functional of Hamprecht, Cohen, Tozer, and Handy (HCTH).[34] For small model compounds $(CH_3)_2SnCl_2$, $(CH_3)_2SnCl_2 \cdot H_2O$, $(CH_3)_2Sn(SCH_3)_2$, and $(CH_3)_2Sn(SCH_3)_2 \cdot H_2O$, full optimizations were carried out both in the gas phase and within the polarized continuum model (PCM) self-consistent reaction field (SCRF) formalism for aqueous solution.[35] Two different basis sets were employed for geometry optimization. The smaller basis set, designated B1, combines the MIDI! basis set[36] for H, C, N, O, and S atoms with the Stuttgart valence-double-ζ effective-core-potential (ECP) basis[37,38] for Cl and Sn and the 6-31G(d) basis[39] for Si (used only for computations of $(CH_4)_3Si$ as an NMR standard). The larger basis set, designated B2, combines the 6-311G(d) basis set[39] for H, C, O, Si, S, and Cl atoms with the Stuttgart valence-double-ζ ECP basis for Sn[37,38] augmented with a single d polarization function having an exponent of 0.15.

To model the geometry of the metal center, the starting conformation of the SNN-PEP/DMT complex was chosen to be the minimized average NMR structure from the ensemble of conformers with the C and N terminal residues replaced by glycine residues (GLGCWCYLG). Geometry optimization was carried out first in the gas phase, employing basis set B1. The optimized structure obtained in the gas phase without distance constraints satisfied all of the experimentally determined dipolar contacts with the exception of the Y7—Hϵ/DMT-methyl proton ROE. On the basis of the experimental data, a single constraint was added holding this distance to 4.6 Å. Subsequent gas-phase optimization led to a final structure that satisfied all ROE constraints. Partial optimizations of this peptide model using PCM formalism had little effect on the gas-phase geometry derived from aqueous solvation. Because numerical noise associated with the SCRF model made it difficult to definitively assign geometric convergence to any specific structure, we do not report here a "final" solvated structure. No attempts were made to determine the free peptide random-coil structures with density functional theory, as the available number of such structures is far too large to permit any reasonable characterization of conformational space at this level.

NMR chemical shift and spin—spin coupling constant calculations employed the one-parameter hybrid exchange-correlation functional of Perdew, Burke, and Enzerhof (PBE1PBE).[40,41] Calculations were carried out both with and without inclusion of aqueous solvation at the SCRF level (in the latter instance, geometries optimized both in the gas-phase

and including SCRF solvation effects were considered). Two different basis sets were employed. For faster calculations, basis set B3 was defined as the 6-31G(d) basis set on H, C, N, O, S, and Si, and the polarized valence-double-ζ basis set of Godbout et al.[42] for Cl and Sn. For more accurate calculations, basis set B4 defined as the IGLO—III basis set of Kutzelnigg et al.[43] was employed for all atoms other than Sn. For Sn, the basis set of Godbout et al.[42] was fully decontracted for all basis functions except for the tightest contracted basis function for each angular momentum quantum number (basis set B4 may be found in the Supporting Information). Chemical shifts are reported relative to Me_4Si for ^1H and ^{13}C and relative to Me_4Sn for ^{119}Sn. Geometries and NMR data for these reference molecules were computed at precisely the same level of theory as that employed for the models.

ESI—MS of SNN-PEP-Y7F. ESI—MS of SNN-PEP-Y7F with and without organotins was analyzed on a ThermoFinnigan LCQ ion trap mass spectrometer equipped with an electrospray ionization interface (ThermoFinnigan, San Jose, CA). Alkyltin compounds dissolved in ethanol were added to the peptide solution and incubated for ~1 h before analysis. The peptide/organotin complexes were then diluted 20 times with 50:50 MeOH/H_2O, 0.2% acetic acid mixture to a final concentration of ~30 μM peptide. Samples were injected at a flow rate of 10 μL/min and detected using a positive ion mode.

Results

1D-^1H NMR of SNN-PEP Titrated with TMT and DMT. The peptide titrations with both TMT and DMT were carried out at pH 4.0 and monitored using 1D-^1H NMR spectroscopy. Upon the addition of increasing amounts of TMT, two different populations of peaks are observed for the peptide in the proton spectrum. This is apparent in Figure 1, where the amide and the aromatic portions of the proton spectra are shown. In particular, the appearance of a second species in solution is evident for the Hϵ of W5 around 10.2 ppm, as indicated by arrows in Figure 1. As confirmed by exchange spectroscopy,[44] peak doubling corresponds to the free and alkyltin bound species of the peptide in slow exchange under the NMR time scale. Figure 1E shows the cross correlation between the free and bound species of the peptide carried out at saturating concentrations of TMT. At lower concentrations of TMT, the peptide was predominantly in the free form, but at a ratio of 6:1 [TMT]: [SNN-PEP], the reaction equilibrium was approximately 50:50 between the free and bound peptide (Figure 1A—C). These results are in agreement with the K_d values determined previously using CD spectroscopy.[7] Only a large excess of TMT (greater than 50:1, [TMT]:[SNN-PEP]) drove the reaction equilibrium to the predominantly bound form of the peptide.

The above titrations were repeated with DMT and the ^1H NMR spectra yielded identical resonance patterns, showing two species in a slow exchange corresponding to the free SNN-PEP and the SNN-PEP/DMT complex (Figure 1D). The 1D-^1H spectra of the peptide in the presence of TMT and DMT, respectively were superimposable, confirming our previous CD

(32) Koradi, R.; Billeter, M. and Wüthrich, K *J. Mol. Graph.* **1996**, *14*, 51—55, 29—32.
(33) Boese, A. D.; Martin, J. M. L.; Handy, N. C. *J. Chem. Phys.* **2003**, *119*, 3005—3014.
(34) Hamprecht, F. A.; Cohen, A. J.; Tozer, D. J.; Handy, N. C. *J. Chem. Phys.* **1998**, *109*, 6264—6271.
(35) Tomasi, J.; Mennucci, B.; Cances, E. *J. Mol. Struct. (THEOCHEM)* **1999**, *464*, 211—226.
(36) Easton, R. E.; Giesen, D. J.; Welch, A.; Cramer, C. J.; Truhlar, D. G. *Theor. Chim. Acta* **1996**, *93*, 281—301.
(37) Ingel-Mann, G.; Stoll, H.; Preuss, H. *Mol. Phys.* **1988**, *65*, 1321—1328.
(38) Bergner, A.; Dolg, M.; Kuechle, W.; Stoll, H.; Preuss, H. *Mol. Phys.* **1993**, *80*, 1431—1441.
(39) Hehre, W. J.; Radom, L.; Schleyer, P. V. R.; Pople, J. A. In Wiley: New York, 1986; p 63.

(40) Perdew, J. P.; Burke, K.; Ernzerhof, M. *Phys. Rev. Lett.* **1996**, *77*, 3865—3868.
(41) Adamo, C.; Cossi, M.; Barone, V. *J. Mol. Struct. (THEOCHEM)* **1999**, *493*, 145—157.
(42) Godbout, N.; Salahub, D. R.; Andzelm, J.; Wimmer, E. *Can. J. Chem.* **1992**, *70*, 560—571.
(43) Kutzelnigg, W., Fleischer, U., Schindler, M. In, Diehl, P., Fluck, E., Gunther, H., Kosfeld, R., Seelig, J., Ed.; Springer-Verlag: Berlin, 1991; Vol. 23, p 165.
(44) Lian, L.; Roberts, G. C. K. In *NMR of Macromolecules a Practical Approach*; Roberts, G. C. K., Ed.; Oxford University Press: New York, 1993.
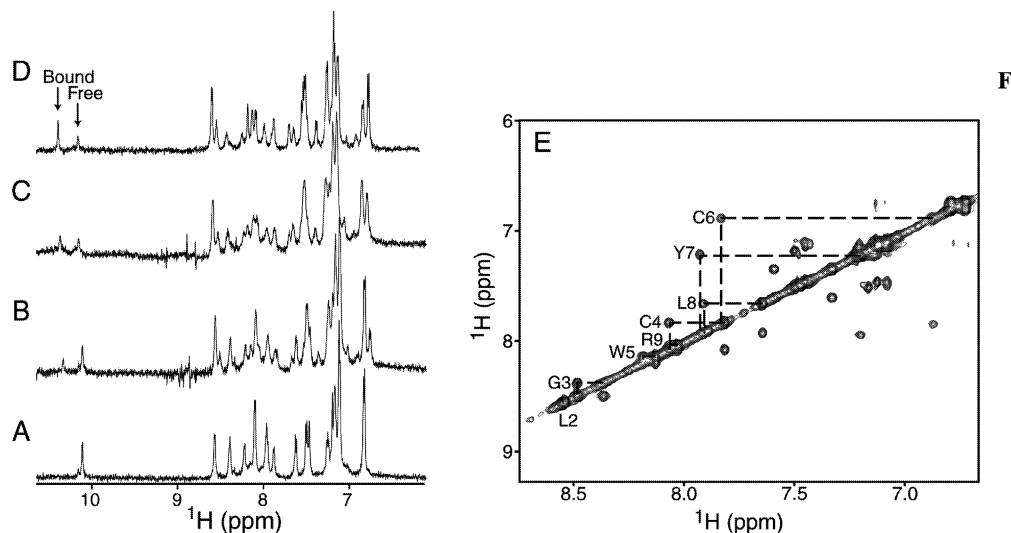
Figure 1. ^{1}H NMR spectra of the SNN-PEP titrated with TMT (A−C) and DMT chlorides (D) showing the presence of two species in solution designated free SNN-PEP and ligand bound SNN-PEP: (A) Free SNN-PEP; (B) 2:1 [TMT]:[SNN-PEP]; (C) 6:1 [TMT]:[SNN-PEP]; (D) 1:1 [DMT]:[SNN-PEP]; (E) NOESY spectrum of the SNN-PEP/DMT complex indicating the slow exchange of the amide protons between the free and bound forms of the peptide.

and ESI−MS results[7] showing that the two complexes formed between TMT or DMT and SNN-PEP were identical. These results support the proposed trialkyltin dealkylation reaction reported previously.[7] In the presence of DMT, however, only a 1:1 ratio of [DMT]:[SNN-PEP] was required to drive the reaction equilibrium to approximately 76% of the bound form, compared to a 20 time excess required in the TMT titration to achieve the same result. Again, these results confirm the higher affinity of SNN-PEP for DMT over TMT.[7] Further addition of DMT did not shift the equilibrium more toward the bound species. At a 7.5:1 ratio of [DMT]:[SNN-PEP], the SNN-PEP/DMT complex precipitated out of solution.

pH Dependence of SNN-PEP-Organotin Complexation. To assess the effects of pH on the ability of SNN-PEP to dealkylate TMT and coordinate DMT, we first formed a 1:1 SNN-PEP/DMT complex, and then systematically adjusted the pH to ~6.5 by the addition of NaOH. A slight increase in the pH from 4.0 to 4.5 resulted in a shift of the equilibrium to predominantly the SNN-PEP/DMT complex (Figure 2C). At a pH of ~6.5, the bound form of the peptide was observable at 90% with a significant decrease in the amount of free SNN-PEP observable (Figure 2D). Since deprotonation of the cysteines at a more neutral pH should increase the reactivity of SNN-PEP for DMT based on the side chain pK_a,[45,46] the increase in affinity for DMT at higher pH indicates that the two cysteines must be directly involved in tin coordination.

Structural Determination of the SNN-PEP/DMT Complex. Since both TMT and DMT form identical complexes with SNN-PEP in solution, we proceeded by determining the structure of the peptide bound to DMT. This allowed us to use equimolar concentrations of peptide and alkyltin, while titration with TMT would require a large excess of ligand complicating the NMR spectra due to the intense methyl resonance at ~1 ppm. Complete resonance assignments for both free and DMT bound SNN-PEP were determined from 2D-[1]H-TOCSY spectra at pH 6.5. In both the free and DMT bound forms, the resonances
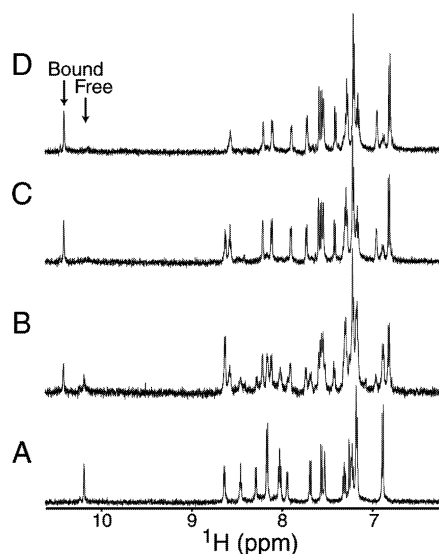
(45) Hynes, M. J.; O'Dowd, M. *J. Chem. Soc.; Dalton Trans.* **1987**, *3*, 563−566.
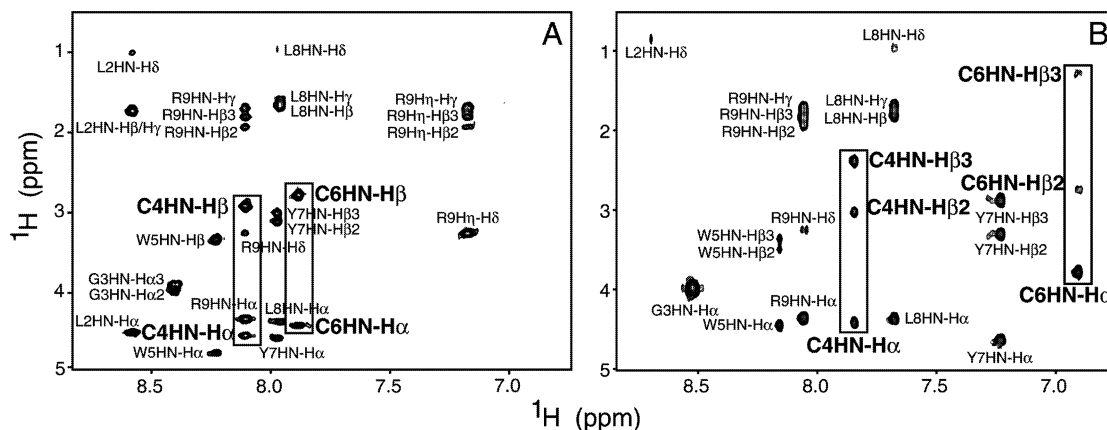(46) Chivers, P. T.; Prehoda, K. E.; Raines, R. T. *Biochemistry* **1997**, *36*, 4061−4066.

Figure 2. ^{1}H NMR spectra of SNN-PEP titrated in a 1:1 concentration ratio with DMT at various pH: (A) Free SNN-PEP (pH 4.0); (B) SNN-PEP/DMT at pH 4.0; (C) SNN-PEP/DMT at pH 4.5; (D) SNN-PEP/DMT at pH 6.5. At a more neutral pH the equilibrium between the free and organotin bound form of the peptides shifts toward predominantly the complexed species.

were well dispersed allowing for straightforward spectral assignment. In the free form, the chemical shifts were representative of a random coil structure (Figure 3A). After titration with DMT, the amide resonances of three residues, including C4, C6, and Y7, shifted considerably going from 8.11, 7.88, and 7.97 ppm to 7.84, 6.90, and 7.23 ppm, respectively (Figure 3B). Moreover, several changes were observed in the aliphatic and the aromatic regions. In particular, the resonances of the Hβ-protons of C4 (2.92 ppm) and C6 (2.78 ppm), which were chemically equivalent in the free peptide, resolved after the addition of DMT and resonated at 3.03 and 2.39 ppm for C4 and 2.75 and 1.26 ppm for C6, respectively. This result clearly implicates both cysteine residues in the coordination of the tin atom and shows that the free rotation of the cysteine side chains is hindered. Furthermore, a dramatic chemical shift of the Y7 Hα and Hβ-protons was also observed, indicating that this

Figure 3. ^{1}H/^{1}H-TOCSY spectra of free SNN-PEP (A) and the SNN-PEP/DMT complex (B). The boxes highlight the significant amide chemical shift differences and Hβ splittings for C4 and C6 upon binding DMT.
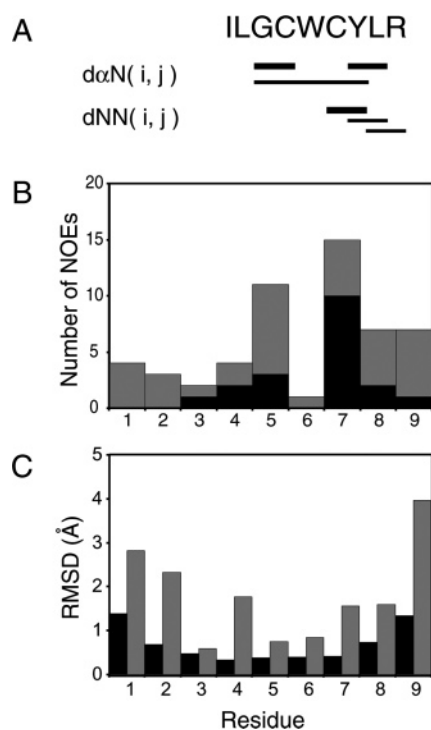

Figure 4. (A) Summary of the ROE connectivities for DMT bound to the 9-residue SNN-PEP. (B) Summation of the intra (black) and inter (gray) ROEs for the complex. (C) RMSD values for the average backbone (black) and side chain atoms (gray) of the 12 lowest-energy structures calculated using X-PLOR.

Table 1. Summary of Structural Statistics for the SNN-PEP/DMT Complex

ROEs and hydrogen bonds		
total ROE	54	
intraresidue ROE	19	
sequential ROE	11	
medium range	30	
H-bond	2	

average energies (kcal mol^{-1})[a]	simulated annealing	refinement
E_{tot}	52 ± 17	-73 ± 15
E_{ROE}	18 ± 10	14 ± 1
E_{bond}	2 ± 1	5 ± 1
E_{angle}	19 ± 4	23 ± 2
$E_{improper}$	3 ± 0.5	5 ± 1
E_{VDW}	10 ± 4	12 ± 5

RMSD (Å)[a]		
backbone	0.77	
side chain	2.11	

average ramachandran angles[a]	Φ (°)	Ψ (°)
C4	-48 ± 5	145 ± 7
W5	-43 ± 3	-34 ± 8
C6	-100 ± 11	18 ± 6
Y7	-121 ± 25	162 ± 10

[a] Average energies, RMSD values to the mean structure and Ramachandran angles were all measured from X-PLOR.[25]

residue is also involved in the stabilization of the ligand. In fact there is an extensive ROE network involving the Y7 side chain upon binding DMT, which is pivotal to the peptide folding (Figure 4).

To determine the three-dimensional structure of the complex, both 2D-NOESY and 2D-ROESY experiments were carried out at different mixing times (see Experimental Section). Due to the small size of the complex, only intraresidue NOEs were observed in the range of mixing times from 100 to 400 ms for the NOESY experiments. On the other hand, several interresidue dipolar contacts were observed and assigned in the ROESY spectra at 350 and 400 ms. A summary of all the dipolar contacts is listed in Table 1 and Figure 4. Some $d_{\alpha N}(i,j)$ and $d_{NN}(i,j)$ interactions were detected including a weak long-range cor-

relation between the G3Hα and Y7HN. In addition, a substantial number of the interresidue ROEs involving protons from both aromatic residues W5 and Y7 were assigned (Figure 4B). These contacts were pivotal for defining the three-dimensional fold of the peptide.

Two independent calculations, both in the presence and absence of the ligand (DMT) in the topology files of the X-PLOR program, were performed. Both calculations yielded a distinctive β-turn fold for the peptide and a similar placement of the aromatic side chains suggesting dipolar contacts were driving the folding of the peptide rather than the β-turn being an artifact of the calculations due to the presence of the alkyltin molecule. In addition to the 54 ROEs, two ROEs between the W5-Hξ2 and the methyl protons of the DMT, and between Y7-Hϵ and the methyl protons of the second methyl group of DMT,
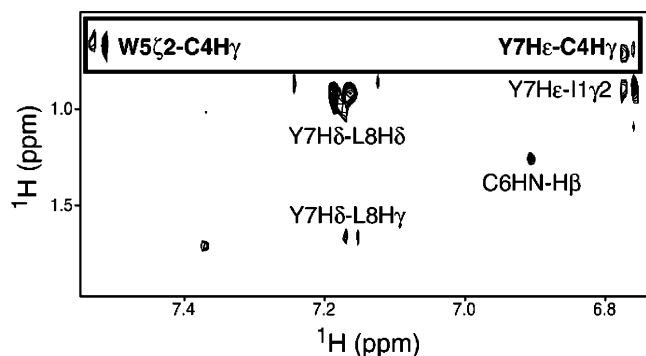
Figure 5. Portion of 2D-ROESY spectrum indicating the ROEs between the aromatic residues and the DMT methyl protons.
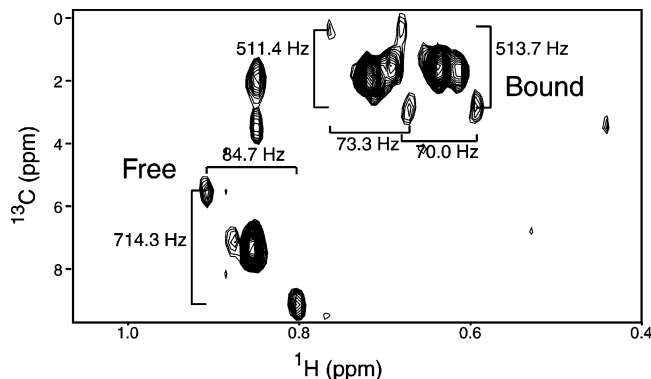

Figure 6. ^{1}H/^{13}C−HMQC of the SNN-PEP/DMT complex indicating the $^1J(^{119}$Sn,^{13}C) and $^2J(^{119}$Sn,^{1}H) couplings for both the free and bound forms of DMT. In the free form the DMT methyl groups are chemically equivalent, but upon binding to SNN-PEP, they are split due to interactions with the aromatic side chains.

were observed (Figure 5). To avoid bias in the peptide folding, these dipolar contacts as well as the hydrogen bonds detected by H/D exchange were not used in the structure calculations. However, the final structures show that the average W5-Hξ2-DMT methyl proton distance is 3.6 ± 0.7 Å, and the Y7-Hϵ-DMT proton from the second methyl group is 4.9 ± 0.8 Å.

$^1J(^{119}$Sn,^{13}C) and $^2J(^{119}$Sn,^{1}H) scalar couplings have been previously used to determine the CH$_3$−Sn−CH$_3$ angle and for assessing the geometry of the tin atom in methyltin compounds.[28,29] We have used this approach to determine the local geometry of the tin center. Figure 6 shows the ^{1}H/^{13}C-HMQC spectrum carried out on a peptide sample titrated with a 1:1 molar ratio of peptide to DMT. The free form of DMT has a single resonance at 7.4 ppm (^{13}C) and 0.9 ppm (^{1}H) with $^1J(^{119}$Sn,^{13}C) and $^2J(^{119}$Sn,^{1}H) of 714.3 and 84.7 Hz, respectively, indicating that the two methyl groups of the free form of DMT are chemically equivalent. In contrast, the methyl resonances in the bound DMT are resolved, indicating that the two methyl groups experience different environments. The chemical shifts of the two methyl groups are 1.9 and 1.6 ppm (^{13}C) and 0.7 and 0.6 ppm (^{1}H), respectively, with $^1J(^{119}$Sn,^{13}C) and $^2J(^{119}$Sn,^{1}H) of 511.4 and 513.7 and 73.3 and 70.0 Hz. Applying Lockhart and Manders equations, we found that the free form of DMT has a CH$_3$−Sn−CH$_3$ angle of 138.7 ± 1.2°, while in the bound form the average angle becomes 121.1 ± 1.4°. These angular values imply that the tin atom has a distorted tetrahedral geometry when complexed with the peptide.

Of the 100 conformers generated with simulated annealing calculations, 81 showed no ROE violations greater than 0.5 Å,

no bond violations greater than 0.5 Å, and no dihedral angle violations greater than 5°. Twelve lowest energy structures were selected for further analysis and their structural overlay is reported in Figure 7A. The peptide backbone folds in a slightly distorted type I β-turn[47,48] that spans from residues C4 to Y7. The average dihedral angles and the relative standard deviations are reported in Table 1. All of the lowest energy conformers are stabilized by two H-bonds found between the carbonyl oxygen of C4 and the amide protons of C6 ($i + 2$) and Y7 ($i + 3$) (Figure 8). These hydrogen bonds have been confirmed experimentally from H/D exchange experiments (see Experimental Section). In the rotated structure reported in Figure 7C, it is possible to observe that the DMT ligand lays on top of the plane defined by the peptide backbone and that both the aromatic rings from W5 and Y7 form a tight cluster with the two methyl groups of DMT.

Density Functional Calculations on Organotin Models. Due to limited solubility of both the peptide and DMT under our experimental conditions, use of ^{119}Sn NMR to ascertain direct information about the tin geometry was not feasible. Consequently, we took a computational approach by performing density functional calculations on several model alkyltin compounds representing DMT in both the free and peptide bound forms. It is well-known that in aqueous environments methyltin salts can be substantially Lewis acidic.[49] Thus, both (CH$_3$)$_2$SnCl$_2$ and (CH$_3$)$_2$SnCl$_2$·H$_2$O were used to model the free DMT chloride species (**1** and **1·H$_2$O**, respectively; see Figure 9). Since the size of the full SNN-PEP/DMT complex makes impractical NMR analysis by standard density functional calculations, the molecules (CH$_3$)$_2$Sn(SCH$_3$)$_2$ and (CH$_3$)$_2$Sn-(SCH$_3$)$_2$·H$_2$O were used to model the core ligand geometry about the metal center (**2** and **2·H$_2$O**, respectively; see Figure 9). The monohydrate species was studied to ascertain the possibility of a water molecule in the tin coordination sphere that may not have been detected by NMR.

The geometries of the two tin species and their respective monohydrates were optimized both in the gas phase and in solution, using the PCM dielectric continuum model[35] to represent aqueous solvation effects. The HCTH density functional[34] was employed for all geometry optimizations, using basis sets of approximately polarized valence-double-ζ (B1) and valence-triple-ζ (B2) quality and an effective core potential for Sn. Choice of the HCTH functional was motivated in part by its demonstrated good performance in the predication of molecular structures including hydrogen bonds or weak bonded interactions;[34] the latter are not necessarily present in the small molecule models but are important in the final model of the peptide/DMT complex. NMR chemical shifts and $^1J(^{119}$Sn,^{13}C) and $^2J(^{119}$Sn,^{1}H) coupling constants were computed for the optimized structures using the PBE1PBE density functional and all-electron basis sets of approximately polarized valence-double-ζ (B3) and full triple-ζ (B4) quality. Use of the PBE1PBE functional for the computation of the NMR data was motivated by its demonstrated good performance for NMR properties.[50]

From the computational results, (CH$_3$)$_2$SnCl$_2$ **1** has a roughly tetrahedral structure (Table 2), while monohydration leads to a

(47) Wilmot, C. M.; Thornton, J. M. *Protein Eng.* **1990**, *3*, 479−493.
(48) Wilmot, C. M.; Thornton, J. M. *J. Mol. Biol.* **1988**, *203*, 221−232.
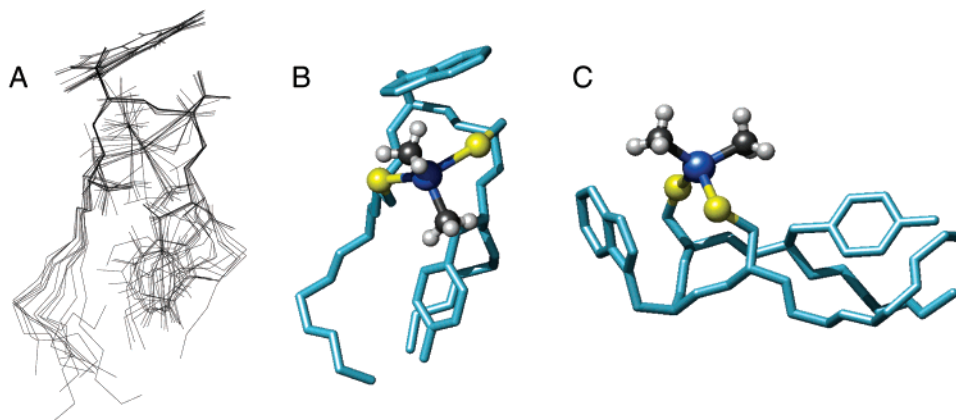(49) Henderson, W.; Taylor, M. J. *Polyhed.* **1996**, *15*, 1957−1964.

Figure 7. (A) Overlap of the 12 lowest energy structures for the SNN-PEP/DMT complex (Only the side chains for residues 4−7 are shown). (B) Single average structure of the peptide complex highlighting the DMT molecule. (C) Rotation of the average structure indicating the aromatic side chain orientations involved in stabilization of the DMT ligand.
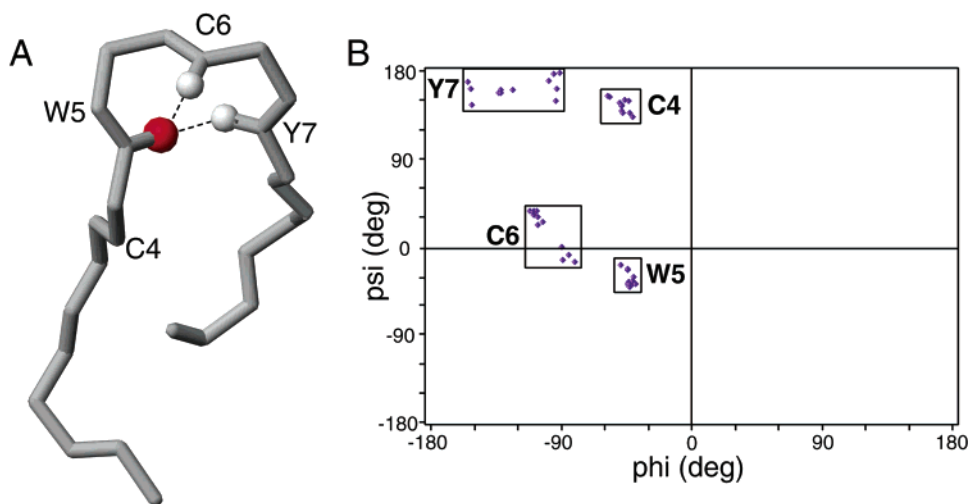

Figure 8. (A) Single average backbone structure of the peptide complex indicating the H-bonds formed during the folding of SNN-PEP by DMT. (B) Ramachandran cluster plot of turn residues (C4−Y7) from the 12 lowest energy structures of the SNN-PEP/DMT complex.

strong Lewis acid/Lewis base interaction between the Sn atom and the water molecule in **1**•H_2O such that the geometry distorts to be more trigonal bipyramidal (Figure 9). This distortion becomes still more pronounced when bulk aqueous solvation is taken into account using the PCM continuum model. One major effect is the opening of the CH_3−Sn−CH_3 bond angle by about 20° compared to the hydrated gas-phase species and another is the increase of the Sn−Cl bond lengths by about 0.2 Å. These geometric changes have large effects on the computed NMR properties. Improving the one-electron basis set also has significant geometric effects and corresponding effects on the NMR data. At the best level of theory (PCM/PBE1PBE/B4// PCM/HCTH/B2), the predicted ^{13}C and ^{1}H chemical shifts of 12.5 and 1.5 ppm compare fairly well with the experimental shifts of 7.4 and 0.9 ppm, respectively. The predicted $^{1}J(^{119}$-Sn,^{13}C) and average $^{2}J(^{119}Sn,^{1}H$) coupling constants of 670.9 and 83.0 Hz for **1**•H_2O also compare well with the measured values of 714.3 and 84.7 Hz, although the $^{1}J(^{119}Sn,^{13}C$) is underestimated by about 44 Hz. Comparing these results to the experimentally determined CH_3−Sn−CH_3 angle for free DMT, it is apparent that the tin atom has a coordinated water molecule. This is shown by the good agreement between the PCM

(50) Cramer, C. J. *Essentials of Computational Chemistry*; Wiley: Chichester, 2002.

calculations of **1**•H_2O (143.7° at B2) and the DMT experimental value of 138.7 ± 1.2°.

Table 3 lists the computational results for $(CH_3)_2Sn(SCH_3)_2$ **2** and a monohydrate; **2** is far less Lewis acidic than the analogous dichloride **1**. Geometry optimizations starting from trigonal bipyramidal monohydrates, both in the gas phase and in continuum aqueous solution, led to ejection of the water molecule from the coordination sphere about tin. Final structures were distorted tetrahedral with the ejected water molecule either left hydrogen bonding to a sulfur atom in the gas phase, or effectively completely dissociated in continuum solvent (distances between sulfur and the nearest water proton exceeding 3.5 Å). Of the two gas-phase hydrogen bonded monohydrates found, **2**•H_2O_a placed the water on a tetrahedral face composed of two methyl groups and one thiomethyl group while **2**•H_2O_b placed the water on a tetrahedral face composed of two thiomethyl groups and one methyl group. The former was found to be lower in energy than the latter by about 4 kcal mol^{-1} both in the gas phase and in continuum solvent, and all computational results hereafter refer only to the lower energy isomer **2**•H_2O_a. Final values for the CH_3−Sn−CH_3 angle calculated from the PCM predictions using B2 for **2** (118.1°) agree well with the experimentally calculated value of 121.1 ± 1.4° determined for the peptide/DMT complex. This result
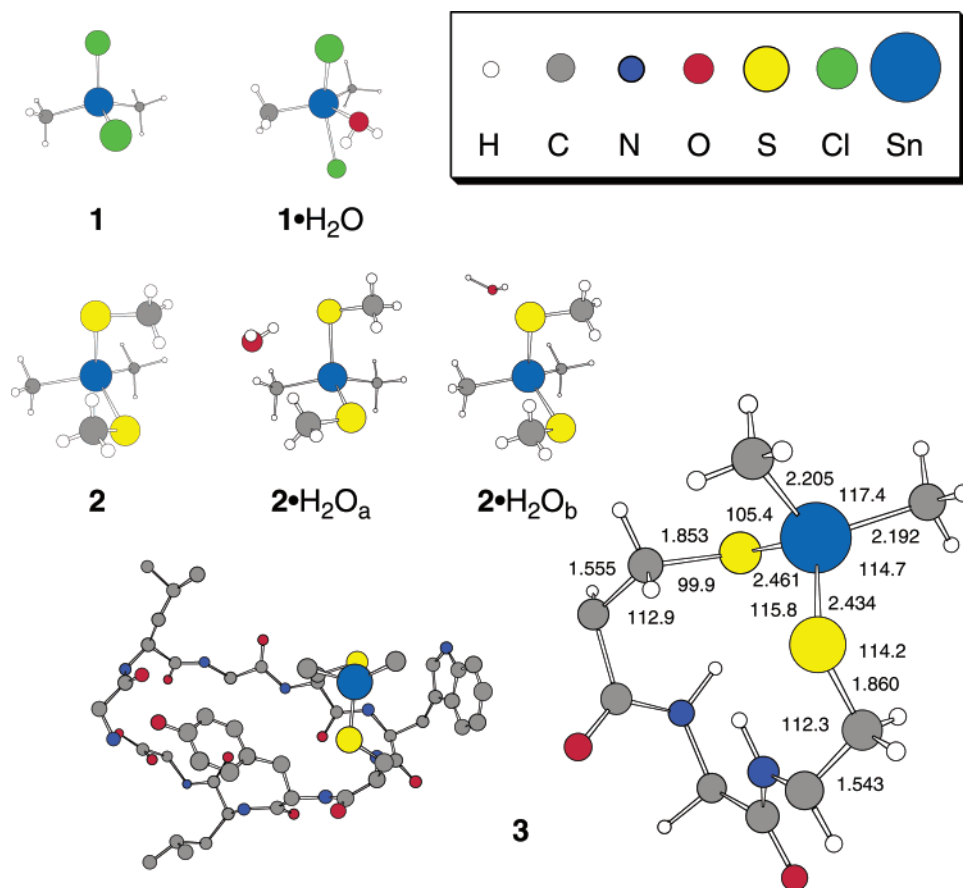
Figure 9. Ball-and-stick optimized structures for various DFT models. Geometric data for **3** are reported for selected bond lengths (Å) and angles (deg) in the expanded, truncated view at right bottom. Hydrogen atoms have been removed from **3** for clarity.

Table 2. Computed Sructural and NMR Spectroscopic Data for Gas-Phase and Aqueous Geometries of **1** and **1**•H_2O^a

	$(CH_3)_2SnCl_2$ (gas)		$(CH_3)_2SnCl_2$•H_2O (gas)		$(CH_3)_2SnCl_2$•H_2O (aq. PCM)	
property	HCTH/B1	HCTH/B2	HCTH/B1	HCTH/B2	HCTH/B1	HCTH/B2
geometric						
r_{SnC}, Å	2.188	2.160	2.189	2.166	2.183	2.158
r_{SnCl}, Å	2.446	2.400	2.634, 2.512	2.558, 2.471	2.663, 2.608	2.625, 2.590
r_{SnO}, Å	n/a	n/a	2.351	2.529	2.246	2.346
θ_{CSnC}, deg	121.6	121.1	132.1	131.9	140.5	143.7
θ_{ClSnCl}, deg	106.7	106.3	152.2	150.7	160.3	160.4
δ, ppm						
^{119}Sn	244.2	230.1	132.8	202.8	52.3 $(-11.4)^b$	101.4 $(36.9)^b$
^{13}C	6.9	4.2	14.7	13.8	16.6 $(14.3)^b$	16.5 $(12.5)^b$
^{1}H (ave)	0.7	0.6	0.9	0.9	1.2 $(1.2)^b$	1.2 $(1.5)^b$
J, Hz						
$^1J(^{119}Sn,^{13}C)$	463.7	474.0	565.6	562.5	613.4 $(668.5)^b$	621.1 $(670.9)^b$
$^2J(^{119}Sn,^1H)$ (ave)	61.	62.	71.	69.	79. $(80.)^b$	80. $(83.)^b$

^{a} NMR data are computed at the PBE1PBE/B3 level unless otherwise indicated. ^{b} NMR data computed at the PBE1PBE/B4 level.

suggests that (a) the $(CH_3)_2Sn(SCH_3)_2$ molecule is an appropriate representation for the tin geometry found in the peptide/DMT complex, and that (b) the peptide/DMT complex forms a stable distorted tetrahedral geometry defined solely by the C4 and C6 sulfhydral groups and the methyl groups as predicted by the experimental NMR data.

The effect of solvation on the geometric and spectral data for $(CH_3)_2Sn(SCH_3)_2$ **2** is almost negligible, with the exception of the values predicted for the ^{119}Sn chemical shift and the

$^1J(^{119}Sn,^{13}C)$ coupling constant. The latter quantity, however, comes into very good agreement with the fully solvated value if the NMR data are computed for the gas-phase structure in the presence of the continuum aqueous reaction field (values found in parentheses and footnoted b in the first two columns of Table 3 compared to values in columns 7 and 8). We note that reoptimization of the *non*-hydrated structure with the PCM model (values found in the third and fourth columns of Table 3) does not lead to very significant changes in the structural

Table 3. Computed Structural and NMR Spectroscopic Data for Gas-Phase and Aqueous Geometries of 2 and 2•H$_2$O$_a$^{a}

property	$(CH_3)_2Sn(SCH_3)_2$ (gas)		$(CH_3)_2Sn(SCH_3)_2$ (aq. PCM)		$(CH_3)_2Sn(SCH_3)_2$•H_2O (gas)		$(CH_3)_2Sn(SCH_3)_2$•H_2O (aq. PCM)	
	HCTH/B1	HCTH/B2	HCTH/B1	HCTH/B2	HCTH/B1	HCTH/B2	HCTH/B1	HCTH/B2
geometric								
r_{SnC}, Å	2.197	2.179	2.190	2.171	2.190, 2.192	2.174, 2.175	2.188, 2.187	2.170, 2.168
r_{SnS}, Å	2.434	2.472	2.446	2.492	2.431, 2.462	2.470, 2.495	2.463, 2.441	2.500, 2.492
r_{SnO}, Å	n/a	n/a	n/a	n/a	3.415	3.637	3.481	4.089
θ_{CSnC}, deg	112.9	115.0	114.2	118.1	114.2	116.0	117.4	118.3
θ_{SSnS}, deg	107.9	108.6	107.3	107.3	106.4	107.5	108.7	107.8
δ, ppm								
^{119}Sn	182.2 (178.1)^b	216.1 (211.9)^b	178.3	227.2	185.6	225.1	190.5	241.9
^{13}C	−2.9 (−2.4)^b	−3.2 (−2.4)^b	−3.2	−3.1	−2.5, −1.2	−2.9, −2.5	−2.7, −2.4	−3.1, −2.8
^{1}H (ave)	0.2 (0.5)^b	0.2 (0.4)^b	0.5	0.4	0.3, 0.5	0.3, 0.4	0.4, 0.5	0.3, 0.4
J, Hz								
$^1J(^{119}Sn,^{13}C)$	391.8 (419.8)^b	396.1 (429.8)^b	423.7	430.3	408.7, 405.7	411.2, 408.2	429.5, 427.6	428.8, 426.7
$^2J(^{119}Sn,^1H)$(ave)	56. (58.)^b	56. (58.)^b	61.	63.	62.	60.	66.	62.

^{a} NMR data are computed at the PBE1PBE/B3 level unless otherwise indicated. ^{b} NMR data accounting for aq. SCRF reaction field but holding geometry fixed at gas-phase optimum.

and NMR data compared to the single-point SCRF model at the gas-phase geometry (values found in parentheses and footnoted b in the first two columns of Table 3.

Density Functional Calculations on the SNN−PEP/DMT Complex. Based on the observations for the $(CH_3)_2Sn(SCH_3)_2$ model **2**, geometry optimization of the peptide GLGCWCYLG/ DMT complex **3** starting from the minimized average NMR structure of the ILGCWCYLR/DMT complex was performed at the HCTH/B1 level (884 basis functions). A single ROE constraint was imposed on the HCTH/B1 gas-phase optimization (see Experimental Section) and the final optimized structure was observed to satisfy all measured ROE constraints. Key geometric details for the peptide **3** may be found in Figure 9. As further geometry optimization with a larger one-electron basis set like B2 was not practical for the peptide, we next computed NMR data for the $(CH_3)_2Sn(SCH_3)_2$ fragment **3**$_{trunc}$ derived from replacing the cysteine backbone carbon atoms with hydrogen atoms and setting the new C−H bond lengths to 1.1 Å.

The predicted values of $^1J(^{119}Sn,^{13}C)$ for **3**$_{trunc}$ at the PCM/ PBE1PBE/B4 level are 465.6 and 473.2 Hz, which compare reasonably well with the measured peptide values of 511.4 and 513.7 Hz, especially given the many simplifications imposed on the theoretical model. An alternative computation that we may consider is to use eq 2. Given the predicted CH$_3$−Sn− CH$_3$ bond angle of 117.4° in **3** (Figure 9), we determine the expected $^1J(^{119}Sn,^{13}C)$ value to be 478.2 Hz. The agreement between this prediction and the direct computation from the DFT probability density for **3**$_{trunc}$ provides some validation of the direct computational protocol, and the underestimation of $^1J(^{119}Sn,^{13}C)$ from DFT is consistent with the analogous comparison for DMT, where a 44 Hz underestimation was observed (see above). For the $^2J(^{119}Sn,^1H)$ coupling constants, DFT predicts values of 54.8 and 61.2 Hz for **3**$_{trunc}$ compared to experimental values for the full peptide of 70.0 and 73.3 Hz. Inspection of Table 3 indicates that geometric relaxation associated with the better basis set B2 combined with taking into account aqueous solvation tends to increase predicted coupling constants for analogous **2** by 5 Hz or so, which would improve agreement between theory and experimental data

somewhat. In DMT, theory also underpredicts experiment (83.0 vs 84.7 Hz) for $^2J(^{119}Sn,^1H)$, albeit by a smaller margin than for **3**$_{trunc}$. Finally, DFT predicts ^{13}C chemical shifts of −5.7 and −4.4 ppm for the methyl group carbon atoms on tin in **3**$_{trunc}$. The agreement with experiment (1.9 and 1.6 ppm) is less good for this quantity than for the coupling constants, but is still reasonable, and is qualitatively correct, by comparison to experiment, in predicting an upfield shift of these signals compared to those in uncomplexed DMT. With respect to predicted ^{1}H chemical shifts, DFT predicts values of 0.4 and 0.2 ppm for **3**$_{trunc}$, respectively, which are again somewhat upfield of the observed values of 0.7 and 0.6 ppm.

There are many possible sources of error in the DFT predictions for the peptide model. Those issues associated with basis-set incompleteness and aqueous solvation have been explicitly discussed. One point that we have not yet addressed is that relativistic effects are unlikely to be negligible for the Sn nucleus, especially with respect to predictions of ^{119}Sn chemical shift. While we have included relativistic effects in the optimization of our molecular geometries through the use of a relativistic effective core potential for Sn, it is much more difficult to include relativistic effects in NMR calculations, and as a result we have not evaluated predicted ^{119}Sn chemical shifts at all. However, the relatively good agreement between theory and experiment for **1**•H$_2$O and DMT, for NMR spectral data *other* than ^{119}Sn chemical shifts suggests that neglect of relativistic effects is not a major issue for these other quantities.

Spectroscopic Analysis of SNN−PEP Variants with Alkyltin Salts. To map the residues crucial for binding and dealkylation, we synthesized three variants of SNN-PEP, where cysteines 4 and 6 were replaced by serines (C4S, C6S), and tyrosine 7 was replaced by phenylalanine (Y7F) and monitored their binding with different organotin compounds using NMR spectroscopy and ESI−MS. Previously, we showed that after removing one of the cysteines, there was no dealkylation of the trialkyltin compounds.[7] Our NMR investigation on the C4S- and C6S-SNN-PEP variants titrated to an excess with TMT (50:1 ratio [TMT]:[peptide]) and DMT resulted in no perturbation of the chemical shifts. The 2D-TOCSY spectra of the C4S-

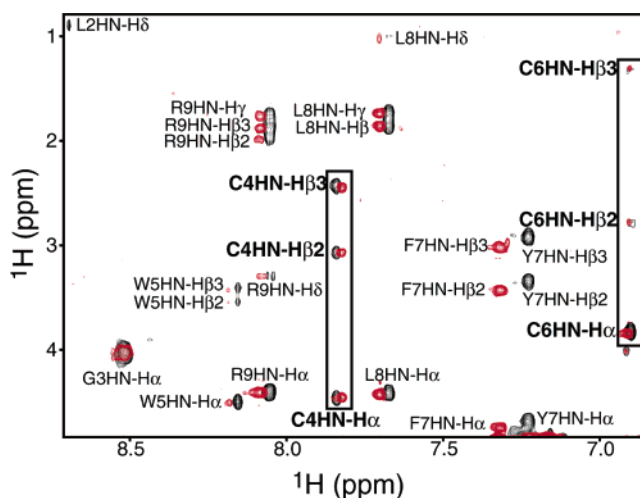**Table 4.** ESI−MS Fragments for Y7F-SNN-PEP Titrated with Various Alkyltin Compounds

	expected (m/z)	observed (m/z)	complex formed
SNN-PEP-Y7F	1110.4	1109.5	Y7F-SNN-PEP
Y7F-SNN-PEP + TMT	1273.3	1257.4	Y7F-SNN-PEP/DMT
Y7F-SNN-PEP + DMT	1258.3	1257.4	Y7F-SNN-PEP/DMT
Y7F-SNN-PEP + TET	1315.4	1285.4	Y7F-SNN-PEP/DET
Y7F-SNN-PEP + DET	1286.3	1285.4	Y7F-SNN-PEP/DET
Y7F-SNN-PEP + TPrT	1357.5	1313.4	Y7F-SNN-PEP/DPrT
Y7F-SNN-PEP + TBT[a]	1399.54	ND	ND
Y7F-SNN-PEP + MMT[a]	1314.1	ND	ND

[a] ND, nondetectable.
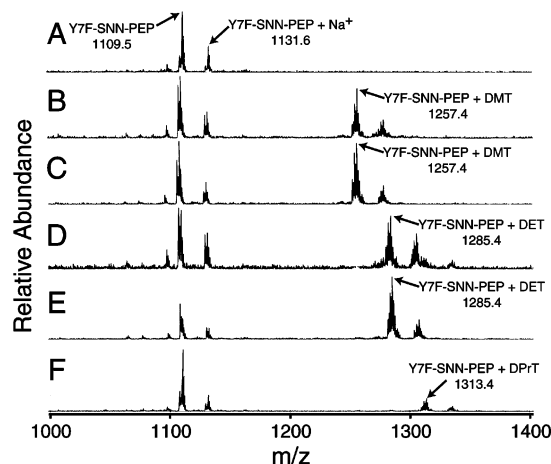
Figure 10. ESI−mass spectra of Y7F-SNN-PEP (m/z 1109.4) (A); Y7F-SNN-PEP/TMT titration (B); Y7F-SNN-PEP/DMT titration (C); Y7F-SNN-PEP/TET titration (D); Y7F-SNN-PEP/DET titration (E); and Y7F-SNN-PEP/TPrT titration (F). Titrations of the peptide with trialkyltin compounds resulted in formation of the respective Y7F-SNN-PEP/SnR₂ complex (where R = methyl, ethyl, propyl). The peak at m/z 1131.5 as well as shoulder peaks of the complexes are plus a Na⁺ ion.

Figure 11. Overlay of the 2D-^{1}H/^{1}H TOCSY spectra for the SNN-PEP/DMT complex (black) and the Y7F-SNN-PEP/DMT complex (red). After binding DMT, the structural changes for both peptides are identical suggesting the Y7F-SNN-PEP variant forms the same β-turn as SNN-PEP when bound to DMT.

and C6S-SNN-PEP variants free and complexed to DMT were superimposable, proving unequivocally that both cysteines are necessary to bind and dealkylate trialkyltin compounds (data not shown).

As discussed above, upon the addition of DMT, a substantial chemical shift change in the peptide Y7 amide resonance was observed. We wanted further evidence to indicate that this chemical shift change was due to the ROE network involving Y7 and not to possible coordination of the side chain hydroxyl oxygen to the tin atom. Thus, to determine the nature and extent of involvement for this residue in stabilizing the tin atom, we used ESI−MS to study the binding of the Y7F variant of SNN-PEP with monomethyltin trichloride (MMT), DMT, DET, TMT, TET, TPrT, and TBT. As in the case of SNN-PEP, ESI−MS spectra of Y7F-SNN-PEP in the presence of TMT, TET, and TPrT showed the m/z of the free peptide (1109.5) plus the respective dialkyltin cation (Table 4 and Figure 10). Analyses of Y7F-SNN-PEP in the presence of DMT and DET were used as controls to verify formation of the peptide/dialkyltin complexes. The formation of TBT or MMT complexes with Y7F-SNN-PEP was not observed. Thus, these experiments prove that after changing the tyrosine to a phenylalanine, the reactivity of the peptide toward the organotin compounds under investigation was not altered, excluding possible involvement of the tyrosine hydroxyl in the reaction.

Moreover, 2D-TOCSY experiments on the free Y7F-SNN-PEP and Y7F-SNN-PEP/DMT complex were utilized to deter-

mine the fold of the peptide variant compared to that of SNN-PEP. The spectra of the free Y7F-SNN-PEP and SNN-PEP were almost superimposable. The addition of a 1:1 concentration ratio of DMT to Y7F-SNN-PEP resulted in distinctive chemical shift changes of C4, C6, and F7. These chemical shift changes coincide with the changes observed in SNN-PEP upon coordinating DMT. The TOCSY spectra for both peptides bound to DMT are overlapped in Figure 11, showing that the overall fold of both peptides is identical. In addition, a ROESY spectrum on the Y7F-SNN-PEP/DMT complex also indicated F7 had the same ROE connectivities through its aromatic protons as were observed for Y7 in SNN-PEP. In sum, these findings show that both cysteines are necessary and sufficient to bind and dealkylate trialkyltin compounds up to three carbons in length, and that the peptide folds and coordinates the tin(IV) atom independently from the Y7 hydroxyl group.

Discussion

Given the significant role of organotins in pollutions and toxicology,[51,52] the literature concerning their binding to biological macromolecules is rather scarce. Most studies focus on organotin interactions with hemoglobins, identifying heme groups as well as histidine and cysteine residues in the direct coordination of trialkyltin compounds.[53−59] Recently, attention has also been focused on the reactivity of these groups toward organotins. In particular, cysteine residues have been implicated in the progressive dealkylation (or speciation) of organotin compounds in both bacteria and mammals,[6,12,17,60,61] with a mechanism similar to the cysteine-catalyzed degradation of

(51) Fent, K. *Crit. Rev. Toxicol.* **1996**, *26*, 1−117.
(52) Champ, M. A. *Sci. Total Environ.* **2000**, *258*, 21−71.
(53) Siebenlist, K. R.; F., T. *Biochem. J.* **1986**, *233*, 471−477.
(54) Celis, H.; Escobedo, S.; I., R. *Arch. Biochem. Biophys.* **1998**, *358*, 157−163.
(55) Aldridge, W. N.; W., S. B. *Biochem. J.* **1970**, *118*, 171−179.
(56) Barry, M. E.; Aldridge, W. N. *Biochem. J.* **1977**, *163*, 583−589.
(57) Rose, M. S.; Lock, E. A. *Biochem J.* **1970**, *120*, 151−157.
(58) Rose, M. S. *Biochem. J.* **1969**, *111*, 129−137.
(59) Zolese, G.; Gabbianelli, R.; Caulini, G. C.; Bertoli, E.; Falcioni, G. *Proteins* **1999**, *34*, 443−452.
(60) Misra, T. K. *Plasmid* **1992**, *27*, 4−16.
(61) Gadd, G. M. *Sci. Total Environ.* **2000**, *258*, 119−127.

alkyllead and alkylmercury compounds.[3,62] Walsh and co-workers have provided very convincing evidence that thiols located in the active site of the enzyme MerB from the bacterial mercury detoxification system[63,64] are able to bind and dealkylate organotin salts,[65,66] explaining why bacteria resistant to organotins also thrive in the presence of organomercury compounds.[67] A similar mechanism has been proposed for the speciation of organomercurial compounds in humans, where dithiols have also been identified as responsible for carrying out this dealkylation reaction.[68] The data presented here complement and support the conclusions of these previous studies, emphasizing the importance of dithiols in structural proteins and enzymes for both coordinating the tin atom and dealkylating TMT to DMT. The CXC motif is widely represented among metalloproteins and, when engineered in linear peptides, is able to coordinate a variety of different metal ions, including Cu^{2+}, Cd^{2+}, Ni^{2+}, and Hg^{2+}.[18] Although this motif is necessary and sufficient for binding and dealkylating short chain alkyltin compounds, further studies will be needed to assess whether other metal binding motifs including dithiols (for instance, CXXC) may carry out the same tin chemistry.

In addition to the chemistry carried out by dithiols, our studies emphasize the ability of DMT to nucleate a stable β-turn structure. This small organic molecule acts as a "molecular clip", binding with relatively high affinity to the sulfydril groups of the two cysteines and stabilizing a β-turn conformation of the peptide backbone. The two aromatic side chains W5 and Y7 that are positioned above and below the central tin atom further stabilize this conformation in a manner similar to potential antitumor dipeptide/dimethyltin complexes.[69] β-turns have been identified as critical motifs for metal ion recognition and peptide stability.[70,71] Therefore, the nucleation of a β-turn structure by DMT may have critical structural significance for the mechanism of toxicity mediated by SNN. One of the current hypotheses formulated by Billingsley and co-workers is that TMT chloride binding to SNN induces a specific conformation that is recognizable by a protein target (14-3-3ζ), thus activating the neuronal apoptosis cascade.[15] On the basis of the peptide model, it is conceivable that the SNN CXC motif binds alkyltin compounds through the vicinal cysteines, forms a β-turn, and induces a secondary structure further in the flexible region of SNN needed to recruit other proteins involved in the apoptotic cascade, inducing a neurotoxic response. This may explain why SNN is necessary but not sufficient to induce the effective neurotoxicity.[4,5] Finally, metal based "molecular clips" have previously been used to induce short α-helical segments in linear peptides.[72] On the basis of the specificity of this peptide for DMT and the stability of the peptide/DMT complex, DMT may be an alternative route for inducing β-turn structures in polypeptides containing vicinal thiols.

Conclusions

We have reported the first high-resolution NMR study and DFT calculation of the interaction between alkyltin compounds and a biological molecule. Using 1D and 2D-^{1}H NMR, we found that a 9-residue peptide containing a CXC motif extracted from the neuronal protein SNN has no preferred structure, but upon the addition of TMT, dealkylates TMT to DMT, and adopts a unique stable type-I β-turn conformation. The secondary structure of the complex and peptide variant studies indicate that the tin(IV) atom of DMT is coordinated only by the cysteine residues defining the CXC motif, while the aromatic rings orient themselves in such a manner as to provide stabilization for the metal complex. The importance of these findings gives new insights on possible mechanisms of organotin compound toxicity that may induce key conformational changes in essential enzymes and structural proteins. These findings also suggest that DMT can behave as an effective β-turn nucleating covalent linker.

(62) Casida, J. E.; Kimmel, E. C.; Holm, B.; Widmark, G. *Acta Chem. Scand.* **1971**, *25*, 1497−1499.
(63) Begley, T. P.; Walts, A. E.; Walsh, C. T. *Biochemistry* **1986**, *25*, 7192−7200.
(64) Pitts, K. E.; Summers, A. O. *Biochemistry* **2002**, *41*, 10287−10296.
(65) Walts, A. E.; Walsh, C. T. *J. Am. Chem. Soc.* **1988**, *110*, 1950−1953.
(66) Walsh, C. T.; Distefano, M. D.; Moore, M. J.; Shewchuk, L. M.; Verdine, G. L. *FASEB J.* **1988**, *2*, 124−130.
(67) Pain, A.; Cooney, J. J. *Arch. Environ. Contam. Toxicol.* **1998**, *35*, 412−416.
(68) Strasdeit, H.; von Dollen, A.; Saak, W, Wilhelm, M *Angew. Chem.; Int. Ed.* **2000**, *39*, 784−786.
(69) Girasolo, M. A.; Guli, G.; Pellerito, L.; Stocco, G. C. *Appl. Organomet. Chem.* **1995**, *9*, 241−250.
(70) Imperiali, B.; Kapoor, T. M. *Tetrahed.* **1993**, *49*, 3501−3510.
(71) Xing, G.; DeRose, V. J. *Curr. Opin. Chem. Biol.* **2001**, *5*, 196−200.
(72) Kelso, M. J.; Hoang, H. N.; appleton, T. G.; Fairlie, D. P. *J. Am. Chem. Soc.* **2000**, *122*, 10488−10489.